In situ damping identification of plant fiber composites using dynamic grid nanoindentation

Taiqu Liu[1], Yves Gaillard[2], Pauline Butaud[3], Vincent Placet[4], Morvan Ouisse[5]

FEMTO-ST Institute, CNRS/UFC/ENSMM/UTBM, Department of Applied Mechanics, Univ. Bourgogne Franche-Comté, F-25000, Besançon, France

Abstract

Damping properties of plant fiber composites have been quite widely investigated based on macroscale techniques. Considering their heterogeneous and hierarchical microstructure, it is also necessary to study their damping behavior at the microscale to provide better insight into the dissipation origins and mechanisms. This article proposes a characterization of the dynamic mechanical properties of flax/GreenPoxy composites at microscale using dynamic grid nanoindentation technique. Two loading protocols are used: the classical Continuous Stiffness Measurement method (CSM) and a new method called Constant Amplitude Measurement method (CAM). Results show experimental protocols (CAM or CSM) do not have significant effect on storage modulus while they significantly affect the loss factor. The grid nanoindentation technique also provides an interesting map of the viscoelastic properties at the microscale in the cross-section of the composites and the damping contribution of the various components are highlighted.

Keywords: Damping; Natural fibers; Biocomposite; Microstructural analysis

---

[1]E-mail: taiqu.liu@univ-fcomte.fr
[2]E-mail: yves.gaillard@univ-fcomte.fr
[3]E-mail: pauline.butaud@univ-fcomte.fr
[4]E-mail: vincent.placet@univ-fcomte.fr
[5]E-mail: morvan.ouisse@femto-st.fr

1 Introduction

Fiber-reinforced composite materials are getting more attention due to their excellent properties in terms of specific strength, fatigue, and damping [1, 2]. Because of environmental impacts concern, plant fibers are becoming alternative materials on account of their abundant reserves, renewability, low cost, and lightweight [3, 4]. Previous studies indicate that the damping properties of tested plant fiber composites (PFCs) are much higher than those of synthetic fiber composites (SFCs) [5, 6].

Many existing researches have been achieved to investigate the damping properties on various temperature and frequency ranges at macroscale based on Dynamic Mechanical Analysis (DMA) and modal analysis [7, 8]. However, plant fibers are more complex than synthetic fibers. Their heterogeneous microstructure, hierarchical organisation, complex morphology and moisture sensitivity lead to specific and complex static, dynamic, and fatigue behavior, including nonlinearities, couplings and moisture activation [9]. This complex structure, involving a heterogeneous polymeric composition, various cell wall layers and their interfaces as well as a central void (lumen) could also be at the origin of additional energy dissipation mechanisms in plant fiber composites, when compared to more traditional composites. It makes the damping sources more complex to comprehend since they combine with the ones commonly observed in synthetic fiber composites, which are related to the viscoelastic nature of the matrix, the friction at the interface between fibers and matrix, and the inelastic and irreversible behaviors such as plasticity and/or damage [2, 6].

During the past few decades, for plant fibers and plant fiber composites, nanoindentation was successfully used mainly to determine the static mechanical properties [10]. Among other, the static mechanical properties of the flax fiber wall were investigated [11] and the reduced modulus and hardness in the cross-section of flax or sisal fiber composites were explored [12, 13, 14]. Similarly, in-situ measurements of the static mechanical properties of the constituents of hemp/GreenPoxy composites were realised using grid nanoindentation by Perrier et al. [15]. Wood cell walls have also been quite widely characterized using nanoindentation in different environments [16, 17, 18]. When it comes to time-delayed properties, Keryvin et al. [19] determined the viscoelastic properties of flax fibers using nanoindentation creep tests.

Access to time-dependent properties of materials through nano-indentation was already men-

tioned in the paper by Pharr & Oliver in 1992 [20]. Dynamic NanoIndentation (DNI) using harmonic component in the excitation has been proposed by Asif and Pethica [21]. Continuous stiffness measurement is typically performed during the loading portion of the indentation test by superposing an harmonic excitation on the monotonically increasing indenter load. This technique has been quite widely used for different materials and shown to be a powerful technique to measure the local time- or frequency-dependent mechanical properties. As an example, Lu and Shinozaki [22, 23] have developed a precisely controlled piezoelectric microindenter to measure the storage modulus (E') and loss factor ($\tan \delta$) of thin film materials. Herbert et al. [24] compared the complex modulus of PVC (highly plasticized polyvinyl chloride) measured by DNI with that of DMA and results show that the difference is less than 15 %.

However, some limitations were reported in other references. It has been observed that the measured quantities such as storage modulus and loss modulus (E'') are not only influenced by material features, but also by the experimental setup itself. Furthermore, for high-density polyethylene, density has been found to be a sensitive factor on the measured E' and E'', while the harmonic amplitude was shown to have a limited influence on these mechanical properties from 5 to 50 Hz [25]. Kramer et al. [26] suggested that the penetration depth should be less than 10 % of the thickness of the sample to avoid the effect of deformation from the substrate. Besides, Deuschle et al. [27] emphasized that the preparation of the surface has a significant impact on the accuracy of the test results.

Up to now, the existing literature has been mostly focused on damping at macroscale or static mechanics of Plant Fiber Composites (PFCs) at the microscale [6], the present study fills the gap by identifying the damping properties of PFCs at microscale. Meanwhile, an alternative technique called Constant Amplitude Measurement method (CAM) is developed to measure the damping without including the effect of plasticity compared with CSM method. Finally, a map of dynamic mechanical properties on the cross-section of the composites is proposed to show the contribution of each component.

2 Material and methods

2.1 Material and its fabrication

In this work, measurements were realised on a flax/epoxy composite and on pristine epoxy polymer. The neat GreenPoxy (GE) was made using the SR GreenPoxy 56 prepolymer and SD7561 hardener supplied by Sicomin (France). The resin and hardener were mixed following a mass ratio of 100:36 in a mould and then cured in a 'Fontjine Grotnes TPC 321' thermocompression device at 60°C for 16 hours, and then post-cured at 100°C for 1 hour after cooling at ambient temperature for 24 hours.

The unidirectional flax/GreenPoxy composites (FGUD) were manufactured using the unidirectional FlaxTape 110 from LINEO and the SR GreenPoxy 56/hardener SD7561 epoxy system. The composite plate was prepared by hand impregnation and cured at 60°C under a pressure of 3 bar for 1 hour, and then it was post-cured at 130°C for 1 hour [28]. The resulting fiber volume fraction was approximately 47 %.

The GE and FGUD plates were finally laser cutted into coupons with size of $65 \times 13 \times 3.5$ mm^3. All the samples were stored in a climatic chamber with 23°C and 50 % RH for at least 4 weeks after cutting to ensure that they reached their moisture content equilibrium.

2.2 Preparation for nanoindentation tests

FGUD coupons were embedded in a fast curing acrylic resin at ambient temperature. FGUD was mounted following the fiber direction shown in Figure 1 in order to perform the nanoindentation on the transverse cross-section of the composite. After the curing of the acrylic resin, the surface of the embedded specimens was finally polished with 40 nm colloidal alumina suspension.
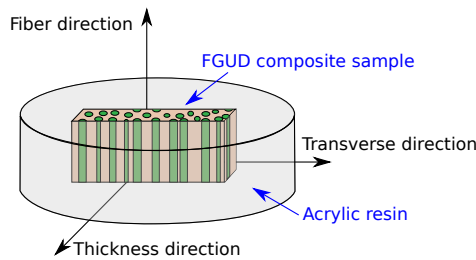

Figure 1: FGUD sample for nanoindentation tests

2.3 Experimental setup

2.3.1 Instrument

All the nanoindentation tests were carried out in a UNHT System (Ultra nanoindentation tester) supplied by Anton Paar. It can be used to characterize the mechanical properties of polymers, films and bio materials at nanoscale on a temperature range from ambient temperature up to 200°C and at relative humidities up to 90 % at ambient temperature. The maximum load of UNHT system is 50 mN with a 3 nN resolution and it can perform a test within 50 μm in depth with a resolution of 0.1 nm. The indenter used in the system was a three-sided pyramid Berkovich tip with a half angle of 65.3° measured from the axis to one of the pyramid flats, as shown in Figure 2 (a). The Young's modulus and Poisson's ratio of the used indenter are 1141 GPa and 0.07, respectively.
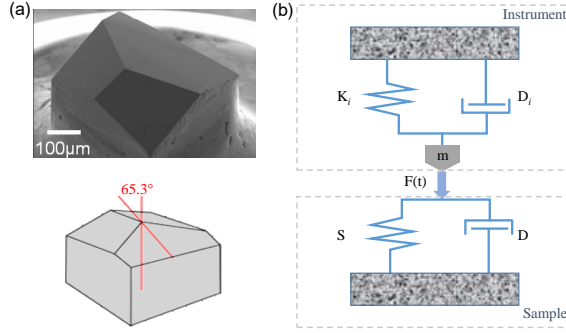

Figure 2: (a) shape of Berkovich indenter, (b) dynamic mechanical model of viscoelastic material in the test system [29]

When considering a homogeneous isotropic material with a linear viscoelastic behaviour, a simple model describing the dynamic behavior of the nanoindentation system is a single-degree-of-freedom spring-mass-damper, as shown in Figure 2 (b) [24]. The spring is composed by a combination of the indentation head and the reference head. A simplified model takes into account only the indentation head. The calculation of storage modulus and loss modulus are determined as follows [24]:

$$\frac{E'}{1 - \nu^2} = (\frac{F_0}{h_0} \cos\delta + m\omega^2 - K_i) \frac{\sqrt{\pi}}{2} \frac{1}{\beta} \frac{1}{\sqrt{A}} \,, \tag{1}$$

$$\frac{E''}{1 - \nu^2} = (\frac{F_0}{h_0} \sin\delta - D_i\omega) \frac{\sqrt{\pi}}{2} \frac{1}{\beta} \frac{1}{\sqrt{A}} \,, \tag{2}$$

where K_i and D_i are the stiffness and damping ratio of the instrument, ν is the Poisson's ratio of the indenter, β is 1.034 for a Berkovich, m is the mass of the indenter. For the instrument used in

this work, the value of K_i, m and D_i are 2346 N/m, 1.9 g and 0.0364 Ns/m, repectively. A is the projected contact area, F_0 and h_0 are force and displacement and δ is the phase difference between force and displacement, $\omega = 2\pi f$ and f is the frequency of the harmonic loading.

2.3.2 Methods for the determination of the viscoelastic properties

• **CSM method**

Dynamic nanoindentation is usually performed with a harmonic force which is superimposed to the monotonic increasing force (CSM method), as shown in Figure 3.

When neglecting the influence of the instrument stiffness and damping, storage modulus (E') and loss modulus (E'') are determined as [24]:

$$\frac{E'}{1-\nu^2} = \frac{F_0}{h_0}\cos\delta\frac{\sqrt{\pi}}{2}\frac{1}{\beta}\frac{1}{\sqrt{A}}, \tag{3}$$

$$\frac{E''}{1-\nu^2} = \frac{F_0}{h_0}\sin\delta\frac{\sqrt{\pi}}{2}\frac{1}{\beta}\frac{1}{\sqrt{A}}. \tag{4}$$

The tangent value of δ is used as loss factor. For tests realized with the CSM method, the phase difference is automatically computed by the nanoindentation software (Indentation 7.2.5®).

• **CAM method**

Although CSM has been widespread used, it should be noted that the quantities measured with CSM method result from elastic, viscoelastic and viscoplastic properties at the same time. Therefore, a
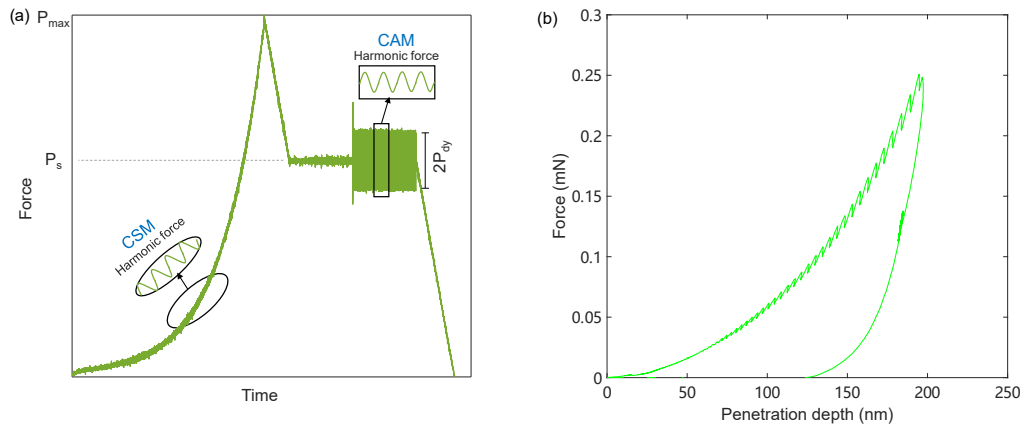

Figure 3: (a) Protocols for viscoelastic properties measurement of CSM and CAM method (b) Typical load-displacement curve

constant amplitude method for damping identification, labeled CAM method, is proposed in this work. The loading path is represented in Figure 3. It consists in first applying monotonic increasing loading and partial unloading phases. The unloading phase is stopped at a certain load level which is then maintained for a given time. Then, a sinusoidal load with constant dynamic and mean amplitudes is applied. After the desired number of harmonic periods at the selected frequency, the load is then monotonically decreased down to zero. In case several frequency values are required, the corresponding excitations can be applied successively with the same mean value. This load-path is similar to the one used in most of the DMA protocols to prevent the measured viscoelastic properties to be interfered by plastic strains.

The labeled 'CSM+CAM' method is used to do the comparison between CSM and CAM methods on the same indentation position to avoid the uncertainty from different measured samples or positions. This procedure starts with a typical CSM analysis and then comes to the same setup using CAM method after the maximum load.

● **Signal processing and viscoelastic properties determination based on CAM method**

A specific signal processing technique was developed to identify the viscoelastic properties from the data recorded during this type of test. The signals of load and displacement as a function of time were extracted from the data files generated by the apparatus. The flow diagram of post-processing for damping identification is drawn in Figure 4. The post-processing starts with an estimation of ω through Fast Fourier Transformation on the whole harmonic signal. Then, a time interval ($2n\pi/\omega$, n=2) is selected to make a nonlinear fitting of load versus time, and displacement versus time signals using the following functions,

$$P(t) = P_0 + Re(\bar{P}e^{j\omega t}), \tag{5}$$

$$\text{with } \bar{P} = P_R + jP_i, \tag{6}$$

$$D(t) = D_0 + Re(\bar{D}e^{j\omega t}), \tag{7}$$

$$\text{with } \bar{D} = D_R + jD_i, \tag{8}$$
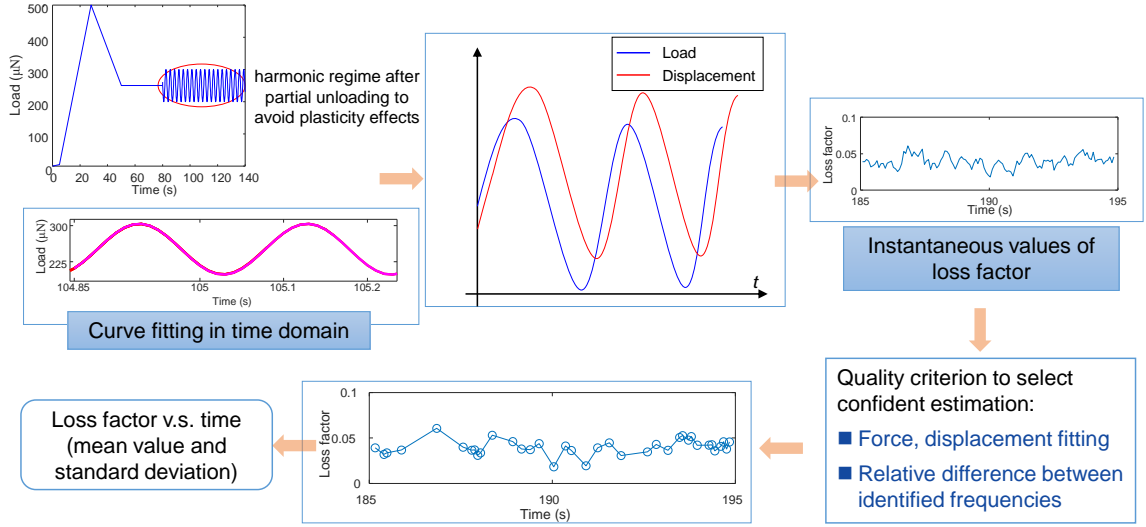
$$\text{and } j = \sqrt{-1}, \tag{9}$$

Figure 4: Post-processing of the load and displacement for damping identification

where $P(t), D(t)$ are the force and displacement time signals, P_0, P_R, P_i, D_0, D_R and D_i are determined by fitting. Then the phase difference δ between the load and displacement can be obtained:

$$\delta = \mathrm{angle}(\frac{\bar{P}}{\bar{\bar{D}}}). \tag{10}$$

The stiffness k_s can be obtained by,

$$k_s = \left| \frac{\bar{P}}{\bar{\bar{D}}} \right|. \tag{11}$$

The storage modulus E' is then determined by:

$$E' = E_s \cos(\delta), \tag{12}$$

where E_S can be determined using the equations 13 and 14 [30], with

$$\frac{1}{E_r} = \frac{(1 - \nu_I{}^2)}{E_I} + \frac{(1 - \nu_S{}^2)}{E_S}, \tag{13}$$

8

E_I and ν_I are Young's modulus and Poisson's ratio of the indenter, E_S and ν_S are the Young's modulus and Poisson's ratio of the sample, respectively, E_r is described as

$$E_{\mathrm{r}} = \frac{\sqrt{\pi}}{2\beta} \frac{S}{\sqrt{A}},\tag{14}$$

where, A is the projected area of the contact surface, β is a constant value related to the shape of the indenter (β=1.034 for Berkovich indenter).

Finally, the time window is shifted and the whole procedure is repeated. This provides the value of loss factor (tan δ) and stiffness over time. Several quality criteria such as residue on load and displacement fitting, relative difference between identified frequencies on load and displacement, and relative difference between identified phases are used for eliminating erroneous points and analyzing the confidence of the values. Finally, the average values is used as the identified loss factor and its standard deviation is used as error value.

For tests realized with the CSM method, the phase difference is automatically computed by the nanoindentation software, which does not provide any uncertainty-related information.

All the nanoindentation tests were carried out in force controlled mode at ambient temperature and 50 % RH. The control of humidity was turned off during measurement to avoid noise effect from the machine.

• **Protocol for unidirectional flax/GreenPoxy composites**

The FGUD sample was tested under 'CSM+CAM method', shown in Figure 3, at room temperature. For 'CSM method', the harmonic load was processed during the loading part with a given dynamic amplitude value of 25 μN until the maximum force of 250 μN was reached. For 'CAM method', the harmonic load was processed after reaching the peak load, and the P_{max}, P_s and P_{dy} quantities were set at a value of 250, 125 and 25 μN, respectively.

In total 144 indent points were carried out on the cross-section of FGUD sample and they were classified in four series (Figure 5 (a)): Fiber zone (points in flax fiber), Matrix zone (points in resin and outside of flax fiber), Fiber-Fiber interface (points cover a surface on neighbouring elementary fiber), Fiber-Matrix interface (points cover a surface on both fiber and resin) [15]. The grid nanoindentation

with CAM method was carried out in 16 × 9 indenter points with an interval space values of around 4 μm in vertical and horizontal axis at 1 Hz and 5 Hz, as shown in Figure 5 (b).
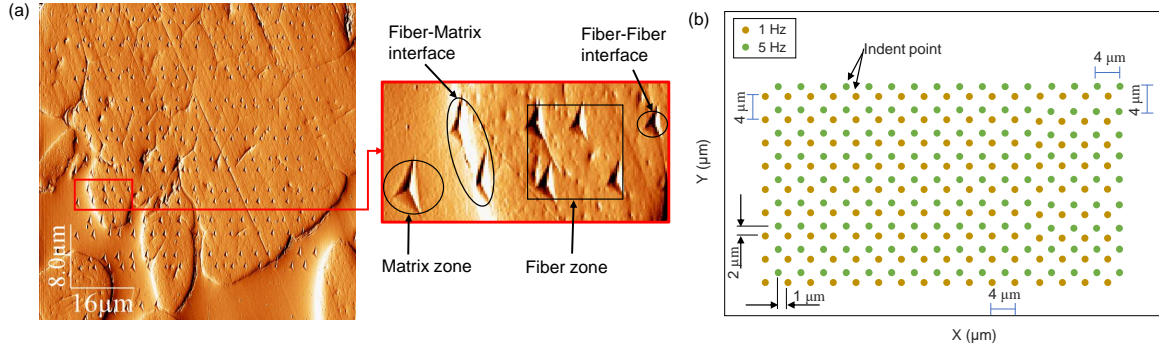

Figure 5: (a) Micro-structure on the cross-section after nanoindentation tests, (b) Schematic diagram of nanoindentation for FGUD using CSM + CAM method at 1 Hz and 5 Hz

• **DMA tests**

DMA tests on pure resin were processed following ASTM D5026-01 under tensile mode using DMA+300 (Metravib) device at ambient temperature. A static displacement of 18 μm and a dynamic displacement of 8 μm were applied to the samples (65 × 10 × 2.5 mm^3). The frequency range for each test were 1-46.4 Hz with 6 values in logarithmic interval and the heating rate was set to 5 °C/min with a 2 minutes hold for each ramp.

3 Results and discussion

3.1 Storage modulus

Grid DNI tests were performed on the cross-section of UD flax/GreenPoxy composites. The storage modulus as a function of the distance between the indent point and fiber edge is shown in Figure 6 (a) and (b). A positive value in distance corresponds to an indent point located in the matrix, while a negative value in distance corresponds to an indent point in the fiber zone. The value of storage modulus varies between 15 and 25 GPa when the indent point is in the fiber wall for both frequency (1 Hz and 5 Hz) no matter what the method (CSM or CAM) is. These values are close to the results measured on hemp/GreenPoxy composites by Perrier et al. [15]. The storage modulus shows a gradual decrease when the indent point is far from the fiber edge (0 μm to 2 μm) due to
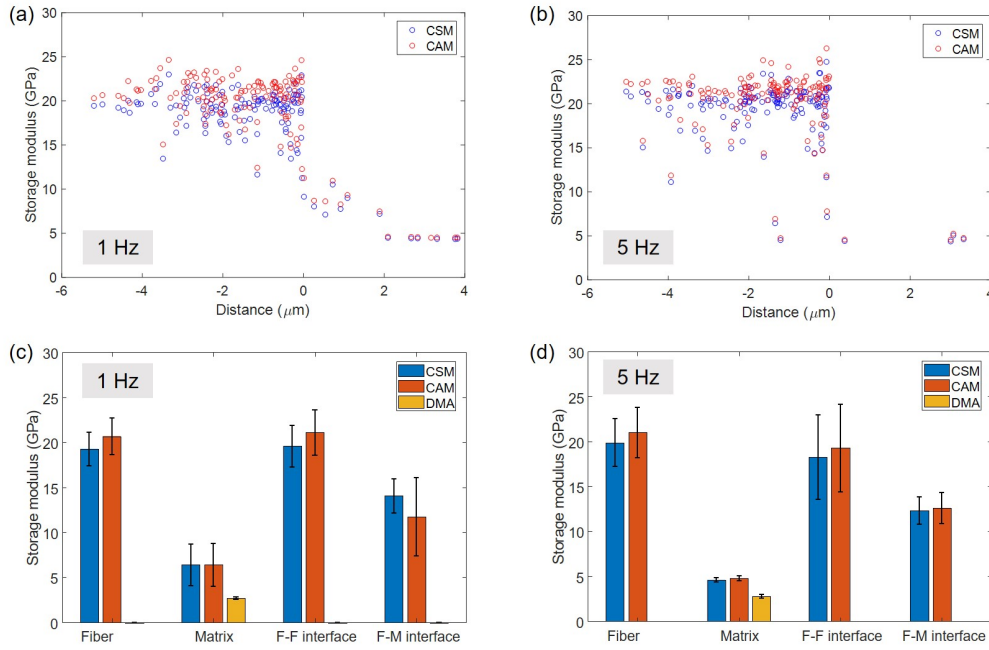
Figure 6: Storage modulus versus distance from fiber edge measured at (a) 1 Hz and (b) 5 Hz, storage modulus of each components at (c) 1 Hz and (d) 5 Hz based on CSM and CAM (The error bar in the figure corresponds to the standard deviation)

the disappeared strengthening of adjacent fibers [15]. Then, the storage modulus is almost constant when the distance is over 2 μm.

The average value of storage modulus in each component including fiber, matrix, Fiber-Fiber (F-F) interface and Fiber-Matrix (F-M) interface obtained by CSM and CAM method is plotted in Figure 6 (c) and (d). The error bar corresponds to the standard deviation. The mean value of the storage modulus in fiber is around 20 GPa and it is close to that measured at F-F interface. For the matrix zone, a value of around 5 GPa is obtained using DNI, while a value of around 2.7 GPa is measured by DMA tests. The differences between DNI and DMA measurements can be attributed to several factors. The first one is related to the uncertainty induced by the surface polishing. The roughness in the near-surface area and the indentation size effect caused by the blunting of the indenter tip at the apex can lead to an overestimate of the modulus [31, 32]. In addition, it exists a large difference in the strain rates and ranges between DMA and DNI. In DNI, measurements are made on a plastified material. Plastic deformations are induced by the high-pressure levels below the indenter. These difference between DMA and DNI is often observed in literature [31, 33]. Above all, in DMA, the mechanical response contains also the ones of the macroscopic defects of the samples

since the entire sample is deformed, while, in DNI, the defects are tried to be avoided.

Considering the standard deviation of the measurements, it can be concluded that the experimental protocol (CSM or CAM) and frequency (1 Hz or 5 Hz) do not have a significant effect on the measured storage modulus. In addition, the values of storage modulus measured in fiber-fiber and fiber-matrix interface may be not accurate due to the influence of the adjacent fiber and the roughness. Overall, the standard deviation in the fibers and in the interfaces is much larger than the one in the matrix, which is in accordance with the literature [15]. This is attributed to the intrinsic variability of the fiber wall and its constituents. Plant fiber has a hierarchical microstructure, and the constituents (cellulose, hemicellulose, lignin, etc) of each micro-layer is also different, which leads to continuous changes in mechanical properties along the cross-section of the fiber [9]. In addition, differences in the growth environment may also cause this variability [34].

3.2 Loss factor

Figure 7 (a) and (b) show the loss factor variation from the distance between indent point and fiber edge. For the measured points at 1 Hz, the value of loss factor in the fiber wall varies between 5 % and 20 % for CSM, while the loss factor is in the range of 2% to 6% when the CAM protocol is used. At 5 Hz, the value is in the range of 5 % to 10 % when using CSM, and between 2% and 6% with CAM. This difference is also found in matrix zone using CSM (around 6 %) and CAM (around 4 %). It points out that the experimental protocol (CSM, CAM) has a significant effect on the measurement of loss factor. The results obtained by CSM have a much higher scattering compared with that identified using CAM. Similar trend can be found when the indent points are in the interface zone. In addition, it is important to notice that the comparison between 1 Hz and 5 Hz, even if measured using the same protocol, may be biased since the indent position is not exactly the same as shown in Figure 5. However, CAM provides similar results both in values and standard deviation between 1 and 5 Hz, which is not the case for CSM.

Figure 7 (c) and (d) show the mean values of loss factor in fiber wall, matrix, F-F interface and F-M interface. The loss factor of matrix obtained by DNI are compared with that tested using DMA method. As shown, the value of loss factor from CAM protocol is close to the one identified by DMA as well as the results in literature [35, 36], whereas the value from CSM protocol is not. The loss
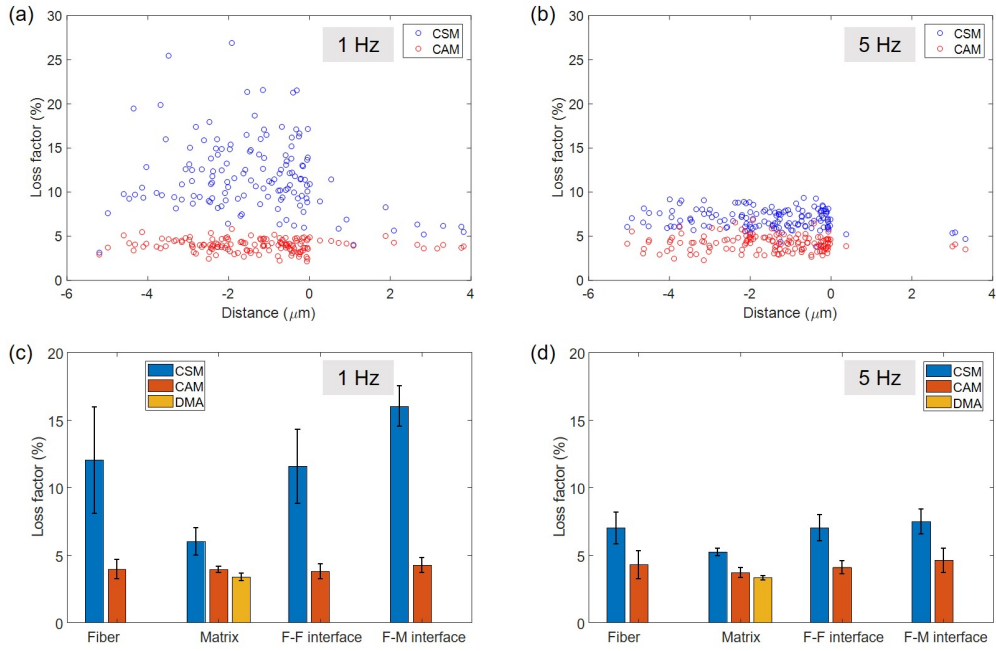
Figure 7: Loss factor versus distance from each fiber edge measured at (a) 1 Hz and (b) 5 Hz, loss factor of each components at (c) 1 Hz and (d) 5 Hz based on CSM and CAM (the error bar in the figure corresponds to the standard deviation)

factor variation in the fiber zones is obviously larger than in the matrix zone no matter what the experimental protocol is. The variability levels observed on the loss factor on fibers, interface and matrix are similar to those obtained for the storage modulus. The underlying physics explaining this are the same. For the fiber wall, the average value of 4 % obtained by CAM is comparable with that of cellulose fibers (4 to 4.5 %) measured by Elsayad et al. [37] by Brillouin spectroscopy. In contrast, the distribution of the loss factor in the matrix zone has a small dispersion level.

The difference in loss factor values measured with CSM and CAM methods is attributed to the method itself. Indeed, in CSM method, the energy dissipated through irreversible mechanisms is taken into account when determining the damping capacity. When using CAM, such mechnisms express themselves in the first loading and unloading phase and then the further determination of the damping capacity is expected to be mostly related to the viscoelasticity of the material. It is thus recommended to use the CAM method when working with this type of materials with complex and inelastic behaviour to ensure a more accurate determination of the damping capacity and viscoelastic parameters.

3.3   Map of the dynamic mechanical behavior of FGUD

In order to show the distribution of storage modulus and loss factor on the cross-section of FGUD more intuitively, the map of storage modulus and loss factor can be plotted using biharmonic spline interpolation. Figure 8 shows an example using the values measured by CSM and CAM at 5 Hz. It shows a clear correspondence for the fiber and matrix zone compared with the cross-section in Figure 5 (a).

This kind of map reflects the gradient of storage modulus and damping from the matrix to the interface and fiber. Besides, the map of loss factor shows the variation between different fibers attributed to the intrinsic variability of fibers (related to maturity and processing effect) in addition to the uncertainty of post-processing in CSM or CAM protocol. Some slight differences in the matrix zone can be interpreted as a difference in local density [25].
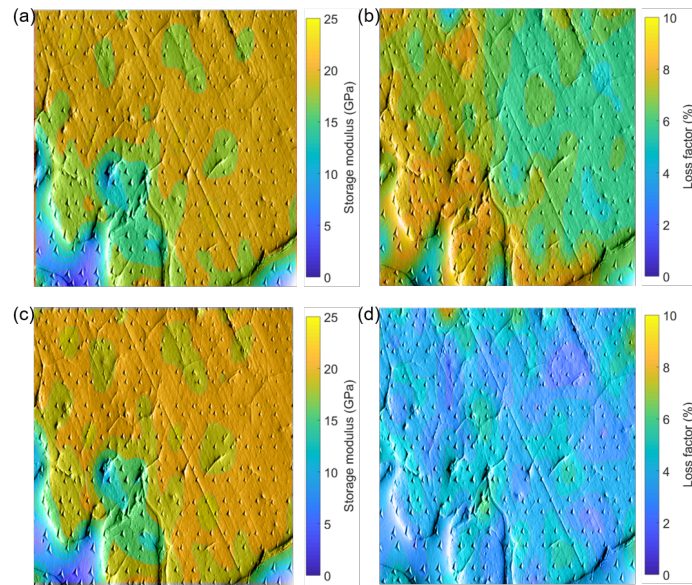

Figure 8: Map on the cross-section based on the results from storage modulus and loss factor at 5 Hz using (a) - (b) CSM and (c) - (d) CAM method on the same sample

Figure 9 provides a graphical representation of the viscoleastic properties along an indentation line in the grid. This line moves across areas containing successively fiber walls and matrix. The transition from the fiber to the matrix, i.e. through the interface, is also clear. The results on the storage modulus are in accordance with the ones reported in literature for hemp/GreenPoxy composites [15]. Interestingly, it can be observed on the map, that the storage modulus and loss factor vary non-linearly within the thickness of the fiber wall. The variations can be due to difference
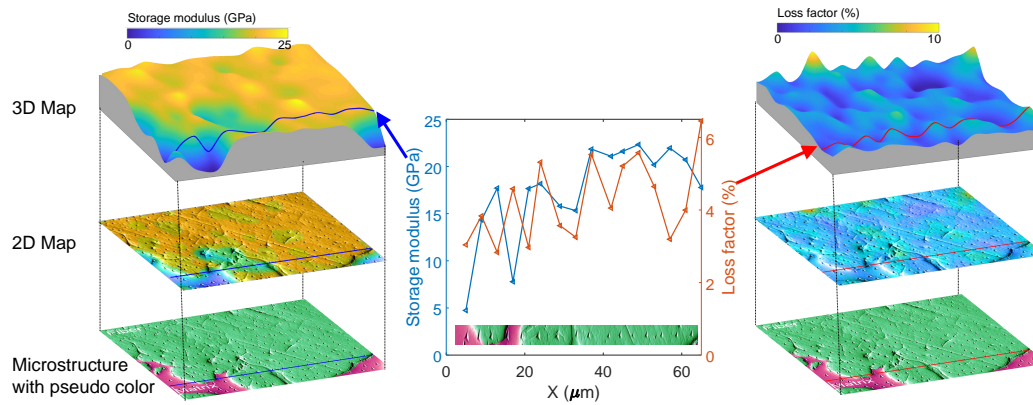
Figure 9: Map of storage modulus and loss factor on the cross-section of FGUD measured by CAM at 5 Hz

in properties between the different cell wall layers [12, 38].

4   Conclusions

This article provides an alternative method for in situ damping identification at microscale. The results obtained with the Constant Amplitude Measurement method (CAM) have been compared to the ones obtained with the usual Continuous Stiffness Measurement method (CSM).

Firstly, the CAM for damping identification is proposed, based on the use of harmonic forces performed at constant mean and dynamic amplitudes after loading and partial unloading of the sample. Then, dynamic mechanical characterization is carried out using 'CSM+CAM' on the cross-section of flax/GreenPoxy composite. Results show that there is no significant influence from experimental protocol (CSM or CAM) on storage modulus. The measurement of storage modulus in interface zone is affected by the adjacent fiber and the roughness.

The loss factor in fiber zone shows a higher scattering than the one in matrix zone due to the intrinsic variability of the fiber wall and its constituents. Results show the measurement of loss factor is highly dependent on experimental protocol compared to that of storage modulus.

The value measured using CAM method can decrease the effect of viscoplasticity compared with CSM. Thus, CAM is recommended to work with the determination of loss factor on the materials with complex and inelastic behavior. Finally, the average loss factor in flax fiber walls measured based on CAM is around 4 %. It is important to note that this kind of comparison should be processed on the same fiber considering the high scattering mechanical properties of plant fiber.

The map of loss factor can show a clear correspondence for each component when compared with the cross-section, which refers to their contribution on energy dissipation.

References

[1] P. Mallick, Fiber-reinforced composites: materials, manufacturing, and design, third edit Edition, CRC Press, Boca Raton, 2007. `doi:10.1201/9781420005981`.

[2] R. Chandra, S. P. Singh, K. Gupta, Damping studies in fiber-reinforced composites - a review, Composite Structures 46 (1) (1999) 41–51. `doi:10.1016/S0263-8223(99)00041-0`.

[3] T. Väisänen, O. Das, L. Tomppo, A review on new bio-based constituents for natural fiber-polymer composites, Journal of Cleaner Production 149 (2017) 582–596. `doi:10.1016/j.jclepro.2017.02.132`.

[4] S. V. Joshi, L. Drzal, A. Mohanty, S. Arora, Are natural fiber composites environmentally superior to glass fiber reinforced composites?, Composites Part A: Applied science and manufacturing 35 (3) (2004) 371–376. `doi:10.1016/j.compositesa.2003.09.016`.

[5] F. Duc, P. E. Bourban, C. J. G. Plummer, J. A. E. Månson, Damping of thermoset and thermoplastic flax fibre composites, Composites Part A: Applied Science and Manufacturing 64 (2014) 115–123. `doi:10.1016/j.compositesa.2014.04.016`.

[6] T. Liu, P. Butaud, V. Placet, M. Ouisse, Damping behavior of plant fiber composites: a review, Composite Structures (2021) 114392`doi:10.1016/j.compstruct.2021.114392`.

[7] N. Saba, M. Jawaid, O. Y. Alothman, M. T. Paridah, A review on dynamic mechanical properties of natural fibre reinforced polymer composites, Construction and Building Materials 106 (2016) 149–159. `doi:10.1016/j.conbuildmat.2015.12.075`.

[8] R. F. Gibson, Modal vibration response measurements for characterization of composite materials and structures, Composites Science and Technology 60 (15) (2000) 2769–2780. `doi:10.1016/S0266-3538(00)00092-0`.

[9] A. Bourmaud, J. Beaugrand, D. U. Shah, V. Placet, C. Baley, Towards the design of high-performance plant fibre composites, Progress in Materials Science 97 (July 2017) (2018) 347–408. `doi:10.1016/j.pmatsci.2018.05.005`.

[10] B. Poon, D. Rittel, G. Ravichandran, An analysis of nanoindentation in linearly elastic solids, International Journal of Solids and Structures 45 (24) (2008) 6018–6033. `doi:10.1016/j.ijsolstr.2008.07.021`.

[11] A. Bourmaud, C. Baley, Nanoindentation contribution to mechanical characterization of vegetal fibers, Composites Part B: Engineering 43 (7) (2012) 2861–2866. `doi:10.1016/J.COMPOSITESB.2012.04.050`.

[12] O. Arnould, D. Siniscalco, A. Bourmaud, A. Le Duigou, C. Baley, Better insight into the nano-mechanical properties of flax fibre cell walls, Industrial Crops and Products 97 (2017) 224–228. `doi:10.1016/j.indcrop.2016.12.020`.

[13] A. Melelli, D. Pantaloni, E. Balnois, O. Arnould, F. Jamme, C. Baley, J. Beaugrand, D. U. Shah, A. Bourmaud, Investigations by afm of ageing mechanisms in pla-flax fibre composites during garden composting, Polymers 13 (14). `doi:10.3390/polym13142225`.

[14] Q. Li, Y. Li, L. Zhou, Nanoscale evaluation of multi-layer interfacial mechanical properties of sisal fiber reinforced composites by nanoindentation technique, Composites Science and Technology 152 (2017) 211–221. `doi:10.1016/j.compscitech.2017.09.030`.

[15] A. Perrier, E. Le Bourhis, F. Touchard, L. Chocinski-Arnault, Effect of water ageing on nanoin-dentation response of single hemp yarn/epoxy composites, Composites Part A: Applied Science and Manufacturing 84 (2016) 216–223. `doi:10.1016/j.compositesa.2016.01.022`.

[16] W. Gindl, T. Schöberl, The significance of the elastic modulus of wood cell walls obtained from nanoindentation measurements, Composites Part A: Applied Science and Manufacturing 35 (11) (2004) 1345–1349. `doi:10.1016/j.compositesa.2004.04.002`.

[17] W. T. Tze, S. Wang, T. G. Rials, G. M. Pharr, S. S. Kelley, Nanoindentation of wood cell walls: Continuous stiffness and hardness measurements, Composites Part A: Applied Science and Manufacturing 38 (3) (2007) 945–953. `doi:10.1016/j.compositesa.2006.06.018`.

[18] M. Eder, O. Arnould, J. W. Dunlop, J. Hornatowska, L. Salmén, Experimental micromechanical

characterisation of wood cell walls, Wood Science and Technology 47 (1) (2013) 163–182. `doi:10.1007/s00226-012-0515-6`.

[19] V. Keryvin, M. Lan, A. Bourmaud, T. Parenteau, L. Charleux, C. Baley, Analysis of flax fibres viscoelastic behaviour at micro and nano scales, Composites Part A: Applied Science and Manufacturing 68 (2015) 219–225. `doi:10.1016/j.compositesa.2014.10.006`.

[20] G. Pharr, W. Oliver, Measurement of thin film mechanical properties using nanoindentation, Mrs Bulletin 17 (7) (1992) 28–33. `doi:10.1557/S0883769400041634`.

[21] S. Asif, J. B. Pethica, Nano-scale viscoelastic properties of polymer materials, Mrs Proceedings 505 (1997) 103. `doi:10.1557/PROC-505-103`.

[22] Y. Lu, D. Shinozaki, Microindentation testing of inhomogeneous microstructures in welded polyethylene, Polymer Engineering & Science 37 (11) (1997) 1815–1824. `doi:10.1002/pen.11831`.

[23] D. Shinozaki, Y. Lu, Micro-indentation relaxation measurements in polymer thin films, Journal of Electronic Materials 26 (7) (1997) 852–858. `doi:10.1007/s11664-997-0262-x`.

[24] E. Herbert, W. Oliver, G. Pharr, Nanoindentation and the dynamic characterization of viscoelastic solids, Journal of physics D: applied physics 41 (7) (2008) 074021. `doi:10.1088/0022-3727/41/7/074021`.

[25] G. Odegard, T. Gates, H. Herring, Characterization of viscoelastic properties of polymeric materials through nanoindentation, Experimental Mechanics 45 (2) (2005) 130–136. `doi:10.1007/BF02428185`.

[26] D. E. Kramer, A. A. Volinsky, N. R. Moody, W. W. Gerberich, Substrate effects on indentation plastic zone development in thin soft films, Journal of Materials Research 16 (11) (2001) 3150–3157. `doi:10.1557/JMR.2001.0434`.

[27] J. Deuschle, S. Enders, E. Arzt, Surface detection in nanoindentation of soft polymers, Journal of Materials Research 22 (11) (2007) 3107–3119. `doi:10.1557/JMR.2007.0394`.

[28] T. Cadu, M. Berges, O. Sicot, V. Person, B. Piezel, L. Van Schoors, V. Placet, S. Corn, R. Léger, L. Divet, et al., What are the key parameters to produce a high-grade bio-based composite? application to flax/epoxy ud laminates produced by thermocompression, Composites Part B: Engineering 150 (2018) 36–46. `doi:10.1016/j.compositesb.2018.04.059`.

[29] B. Fischer-Cripps, Nanoindentation, Springer, 2011.

[30] W. C. Oliver, G. M. Pharr, An improved technique for determining hardness and elastic modulus using load and displacement sensing indentation experiments, Journal of materials research 7 (6) (1992) 1564–1583.

[31] L. Shen, L. Wang, T. Liu, C. He, Nanoindentation and morphological studies of epoxy nanocomposites, Macromolecular Materials and Engineering 291 (11) (2006) 1358–1366. `doi:10.1002/mame.200600184`.

[32] W. D. Nix, H. Gao, Indentation size effects in crystalline materials: a law for strain gradient plasticity, Journal of the Mechanics and Physics of Solids 46 (3) (1998) 411–425. `doi:10.1016/S0022-5096(97)00086-0`.

[33] D. Tzetzis, G. Mansour, I. Tsiafis, E. Pavlidou, Nanoindentation measurements of fumed silica epoxy reinforced nanocomposites, Journal of Reinforced Plastics and Composites 32 (3) (2012) 163–173. `doi:10.1177/0731684412463978`.

[34] C. Goudenhooft, A. Bourmaud, C. Baley, Conventional or greenhouse cultivation of flax: What influence on the number and quality of flax fibers?, Industrial Crops and Products 123 (2018) 111–117. `doi:10.1016/j.indcrop.2018.06.066`.

[35] S. M. Rangappa, J. Parameswaranpillai, K. Yorseng, H. Pulikkalparambil, S. Siengchin, Toughened bioepoxy blends and composites based on poly(ethylene glycol)-block-poly(propylene glycol)-block-poly(ethylene glycol) triblock copolymer and sisal fiber fabrics: A new approach, Construction and Building Materials 271 (2021) 121843. `doi:10.1016/j.conbuildmat.2020.121843`.

[36] K. Yorseng, S. M. Rangappa, H. Pulikkalparambil, S. Siengchin, J. Parameswaranpillai, Accelerated weathering studies of kenaf/sisal fiber fabric reinforced fully biobased hybrid bioepoxy composites for semi-structural applications: Morphology, thermo-mechanical, water absorption behavior and surface hydrophobicity, Construction and Building Materials 235 (2020) 117464. `doi:10.1016/j.conbuildmat.2019.117464`.

[37] K. Elsayad, G. Urstöger, C. Czibula, C. Teichert, J. Gumulec, J. Balvan, M. Pohlt, U. Hirn, Mechanical properties of cellulose fibers measured by brillouin spectroscopy, Cellulose (2020) 1–12`doi:10.1007/s10570-020-03075-z`.

[38] Q. Li, Y. Li, L. Zhou, Nanoscale evaluation of multi-layer interfacial mechanical properties of sisal fiber reinforced composites by nanoindentation technique, Composites Science and Technology 152 (2017) 211–221. `doi:10.1016/j.compscitech.2017.09.030`.